Enhancement of p-Type Dye-Sensitized Solar Cell Performance by Supramolecular Assembly of Electron Donor and Acceptor

Haining Tian[1]*, Johan Oscarsson[2], Erik Gabrielsson[1], Susanna K. Eriksson[3], Rebecka Lindblad[2], Bo Xu[1], Yan Hao[4]*, Gerrit Boschloo[3], Erik M. J. Johansson[3], James M. Gardner[5], Anders Hagfeldt[3], Håkan Rensmo[2] & Licheng Sun[1,4]

[1]Organic Chemistry, Centre of Molecular Devices, Department of Chemistry, School of Chemical Science and Engineering, KTH Royal Institute of Technology, SE-10044 Stockholm, Sweden, [2]Division of Molecular and Condensed Matter Physics, Department of Physics and Astronomy, Uppsala University, SE-751 20 Uppsala, Sweden, [3]Physical Chemistry, Centre of Molecular Devices, Department of Chemistry-Ångström, Uppsala University, SE-751 20 Uppsala, Sweden, [4]State Key Laboratory of Fine Chemicals, DUT-KTH Joint Research Centre on Molecular Devices, Dalian University of Technology (DUT), 116024 Dalian, China, [5]Applied Physical Chemistry, Centre of Molecular Devices, Department of Chemistry, School of Chemical Science and Engineering, KTH Royal Institute of Technology, SE-10044 Stockholm, Sweden.

Supramolecular interactions based on porphyrin and fullerene derivatives were successfully adopted to improve the photovoltaic performance of p-type dye-sensitized solar cells (DSCs). Photoelectron spectroscopy (PES) measurements suggest a change in binding configuration of ZnTCPP after co-sensitization with C60PPy, which could be ascribed to supramolecular interaction between ZnTCPP and C60PPy. The performance of the ZnTCPP/C60PPy-based p-type DSC has been increased by a factor of 4 in comparison with the DSC with the ZnTCPP alone. At 560 nm, the IPCE value of DSCs based on ZnTCPP/C60PPy was a factor of 10 greater than that generated by ZnTCPP-based DSCs. The influence of different electrolytes on charge extraction and electron lifetime was investigated and showed that the enhanced V_{oc} from the $Co^{2+/3+}(dtbp)_3$-based device is due to the positive E_F shift of NiO.

P-type dye-sensitized solar cells (DSCs)[1–10] have attracted intensive interest in the community due to the potential applications in tandem devices[11,12] with n-type DSCs[13] as well as in the artificial photosynthesis systems[14,15]. So far, the highest efficiency of p-type dye-sensitized solar cells is 1.3% obtained by the combination between an organic dye and a cobalt redox couple[16]. In DSCs, the photosensitizer is always one of the crucial components of the devices. To date, some organic as well as inorganic photosensitizers have been developed for p-type DSCs[2–5,12,17–21]. In order to improve the photovoltaic properties of p-type DSCs, the recombination process between injected holes in the valence band (VB) of the p-type semiconductor and reduced photosensitizer should be inhibited as much as possible[4]. This problem can be addressed by judicious design of the photosensitizer, including extension of the conjugated system to increase the distance between the electron acceptor unit and the p-type semiconductor surface. This synthetic approach has been shown to provide a longer lifetime of the charge separated state[12,22]. Recently, a porphyrin dye showed a promising device efficiency up to 11%, a comparable efficiency to classic Ru photosensitizers that are ubiquitous in n-type DSC[23]. These two points were the main motivations for using porphyrin dyes in p-type DSCs. Lindquist and co-workers adopted the meso-tetra(carboxyphenyl) porphyrin (TCPP) for p-type DSCs in 1999[24]. However, at that moment the efficiency of the p-type DSCs based on this porphyrin dye was very unsatisfying, around 0.003%, with the highest incident photon-to-current conversion efficiency (IPCE) value of 0.24% at 540 nm. The poor photovoltaic properties were probably due to the fast hole recombination processes and the quality of the NiO films. Inspired by previous examples of supramolecular interaction between porphyrin and C60 and the fast charge transfer process from porphyrin to C60 derivatives[25–29], a C60 derivative, N-methyl-2-(4′-pyridyl)-3,4-fulleropyrrolidine (C60PPy) was adopted to carry out the formation of the supramolecular photosensitizer with porphyrin dyes on NiO surfaces. The structures of porphyrin dyes (TCPP and ZnTCPP) and C60PPy are illustrated in Figure 1a. Through the
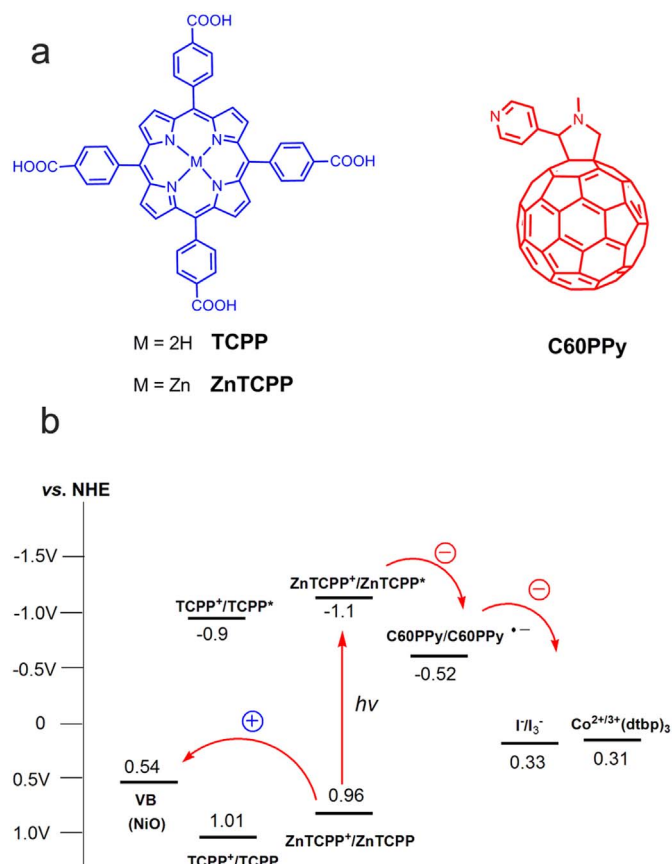
Figure 1 | (a), The structures of ZnTCPP and C60PPy; (b), The potential diagram of the components used in this study.

supermolecular assembly of between ZnTCPP and C60PPy, photovoltaic performance of the DSC was increased by a factor of 4.

Results

Potentials. Figure 1b shows the potential diagram of NiO, TCPP, ZnTCPP and C60PPy as well as I^-/I_3^- and $Co^{II/III}$ tris(4,4′-di-tert-butyl-2,2′-dipyridyl) (herein referred to as $Co^{2+/3+}(dtbp)_3$). The potential of valence band (E_{VB}) of NiO was determined to be 0.54 V vs. Normal Hydrogen Electrode (NHE) at pH 7.0[24]. The potential value of $C60PPy^{•-}$ is estimated to be -0.52 V vs. NHE[30,31]. The $Co^{2+/3+}(dtbp)_3$ redox couple was introduced into the study due to its more negative redox potential, -0.32 V vs. $Fc^{0/+}$, when compared with I^-/I_3^-, -0.30 V vs. $Fc^{0/+}$[32]. $Fc^{0/+}$ has a redox potential of 0.63 V vs. NHE[33]. Thus, the redox potential values of $Co^{2+/3+}(dtbp)_3$ and I^-/I_3^- vs. NHE are calculated to be 0.31 V and 0.33 V, respectively.

The HOMO levels of TCPP and ZnTCPP are 1.01 V[24] and 0.96 V[34] vs. NHE, respectively, well below the energy level of E_{VB} of NiO; this indicates that hole injection from dye into VB of NiO is thermodynamically feasible. The LUMO levels of TCPP and ZnTCPP are -0.9 V[24] and -1.1 V[34] vs. NHE, which are above the energy level of $C60PPy^{•-}$ as well as redox couples. Therefore, porphyrin dye regeneration by $C60PPy^{•-}$ or redox couples are both thermodynamically feasible. Moreover, the substantial difference in energy level between $C60PPy^{•-}$ and the redox couple ($\sim$0.2 V) shows that there is a strong driving force for C60PPy regeneration by the redox couple in the following prepared solar cells.

Photovoltaic and photoelectrochemical properties of devices based on I^-/I_3^-. The photovoltaic properties of DSCs based on different sensitizers under simulated sun light illumination

(100 mW·cm^{-2}) are shown in Table 1. The J-V curves and IPCE spectra of DSCs based on ZnTCPP/C60PPy and ZnTCPP are depicted in Figure 2a–b. From the photovoltaic data in shown in Table 1, the p-type DSCs based on TCPP and ZnTCPP gave the same efficiencies (0.02%). When C60PPy was introduced into the p-type DSCs, the photovoltaic properties of devices based on both TCPP/C60PPy and ZnTCPP/C60PPy significantly improved as compared to that of DSCs solely based on porphyrin dyes. To prove that the enhanced photovoltaic performance of the DSCs based on the porphyrin photosensitizer and C60PPy are not ascribed to decreased porphyrin aggregation, the ubiquitous aggregation inhibitor, chenodeoxycholic acid (CDCA), was introduced into porphyrin DSCs. No improvement in efficiency was observed from the addition of CDCA, which indicates that C60PPy does not primarily act as a de-aggregator in these solar cells. As a consequence, it was considered that C60PPy could form a supramolecular complex with the porphyrin dyes, and in so doing suppress the hole recombination reaction by carrying out a two-step charge transfer process.

The IPCE values of DSCs based on ZnTCPP/C60PPy show significant improvements in efficiency when compared to that of DSCs using ZnTCPP dye alone or with CDCA. The highest IPCE value obtained by ZnTCPP/C60PPy based DSC is 35% at 430 nm. Impressively, at 560 nm, the DSCs based on ZnTCPP/C60PPy gave an IPCE value of 12%, which is more than 10 times higher than that generated by ZnTCPP-based DSCs alone, 1%. Notably, ZnTCPP/C60PPy-based p-type DSCs obtained a much higher efficiency, 0.09%, compared to TCPP/C60PPy-based p-DSCs, which showed an efficiency of only 0.04%. After changing the sensitization order between ZnTCPP and C60PPy, the C60PPy/ZnTCPP device gave an efficiency of 0.05%, which is lower compared to the ZnTCPP/C60PPy device, but still higher than the ZnTCPP device.

Photophysical properties in solution and on NiO surface. From the UV-Vis absorbance spectrum of C60PPy on NiO (Figure S4), it was observed the C60PPy can adsorb to the surface of NiO due to the presence of the pyridine unit acting as an anchoring group[35]. However, the amount on the surface is rather low. The adsorbed C60PPy on NiO surface could form a supramolecular complex with TCPP or ZnTCPP via a π-π interaction between the fullerene and the geometric center on the porphyrins[25,29]. Moreover, for ZnTCPP, the Zn metal center provides the possibility to directly coordinate with the pyridine unit in C60PPy[29,36]. Therefore, these results imply that there could be two different interactions between ZnTCPP and C60PPy; stacking and coordination. For ZnTCPP/C60PPy, these two interactions could exist simultaneously. However, for C60PPy/TCPP, there must be only stacking interaction. From the photovoltaic properties of the solar cells, it seems that both interactions are in favor of improving the photovoltaic performance.

In order to test this theory, UV-Vis absorbance spectroscopy experiments on NiO films sensitized with different compounds were performed (see Figure 3). The absorbance spectrum of the porphyrin

Table 1 | Photovoltaic properties of DSCs based on different sensitizers (Light intensity: 100 mW·cm^{-2}; [b] 3 μm NiO and the electrolyte E1 consisting of 1.0 M LiI and 0.1 M I$_2$ in acetonitrile (AN))

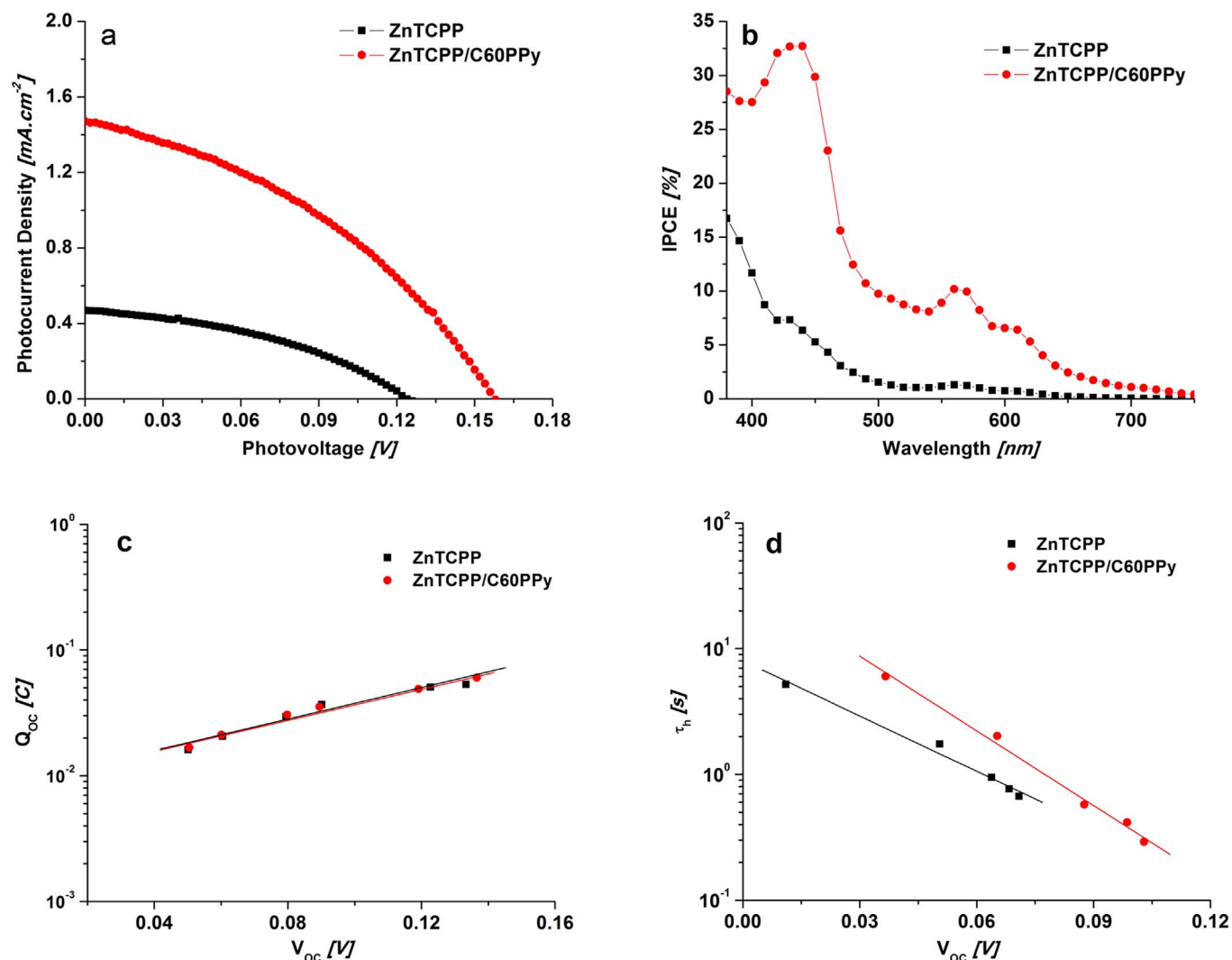| Sample[b]	J_{SC} [mA·cm^{-2}]	V_{OC} [mV]	ff	η [%]
TCPP	0.5	110	0.42	0.02
TCPP/C60PPy	0.8	128	0.39	0.04
ZnTCPP	0.5	120	0.40	0.02
ZnTCPP/CDCA	0.5	114	0.42	0.02
ZnTCPP/C60PPy	**1.5**	**158**	**0.38**	**0.09**
C60PPy/ZnTCPP	1.0	125	0.37	0.05

Figure 2 | *J-V* curves (a) and IPCE spectra (b) of DSCs based on ZnTCPP/C60PPy and ZnTCPP; Extracted charge (c) and hole lifetime (d) as a function of *Voc* for DSCs based on ZnTCPP/C60PPy using E1 electrolyte.

functionalized NiO film containing C60PPy obviously exhibits a red-shift in comparison to that of the pure porphyrin-based NiO film. Comparing with the pure ZnTCPP-sensitized NiO film, introduction of CDCA, 4-*tert*-butylpyridine (TBP) or pure C60 into ZnTCPP-sensitized NiO electrodes changed nothing in the absorbance spectra. The red-shift of the Soret and Q bands of porphyrins have been used as a strong evidence to show the formation of supramolecular interaction with C60 derivatives[37]. The interaction between ZnTCPP and C60PPy resulted in a red-shift of the ZnTCPP absorbance in organic solvent as well (Figure S9). The results strongly suggest that the supramolecular interaction between C60PPy and porphyrin dyes exists on the surface of NiO films.

From the UV-vis absorbance spectra of different ZnTCPP and TCPP sensitized NiO electrodes with/without C60PPy (Figure S5), the ZnTCPP/C60PPy-based NiO film showed a slight red-shift and broadening of the absorbance as compared to the C60PPy/ZnTCPP sample (Figure S5a). However, as shown in Figure S5b, no obvious difference of the final absorbance spectra between TCPP/C60PPy and C60PPy/TCPP was detected. The results probably indicate that not only is there a supramolecular π-π interaction between the adsorbed C60PPy and ZnTCPP in ZnTCPP/C60PPy sample, the coordination between C60PPy and ZnTCPP *via* the pyridine and Zn metal atom could be another supramolecular interaction in ZnTCPP/C60PPy as well[36,37]. The result is well in agreement with

that from photovoltaic tests. A model of supramolecular structure and electron transfer processes on the NiO electrode is demonstrated in Figure 4. The additional coordination of the ZnTCPP/C60PPy sample and the strong electron transfer driving force (Figure 1b)
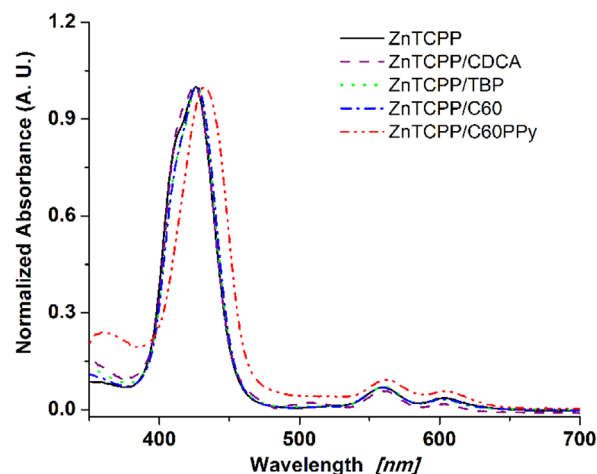

Figure 3 | Absorbance spectra of different ZnTCPP-based samples on NiO films.

between ZnTCPP and C60PPy should be responsible for the higher efficiency obtained by ZnTCPP/C60PPy-based DSCs in comparison with that from TCPP/C60PPy-based DSCs.

Photoelectrochemical measurements were carried out to further study the essential effect of the supramolecular interaction on the photophysical properties of DSCs. From charge extraction measurements, as shown in Figure 2c, no difference was observed in ZnTCPP and ZnTCPP/C60PPy based p-type DSCs, which implies that the introduction of C60PPy in DSCs does not change the position of the VB edge of NiO. However, from photovoltaic measurements, the V_{OC} value, 158 mV, of ZnTCPP/C60PPy-based p-type DSC is higher than that of ZnTCPP-based DSC (120 mV). As shown in Figure 2d, the hole lifetimes (τ_h) of ZnTCPP/C60PPy and ZnTCPP-based DSCs are plotted as a function of V_{OC}. At a given V_{OC}, τ_h of ZnTCPP/C60PPy-based DSCs is much longer than that of DSCs employing ZnTCPP. Therefore, the enhanced V_{OC} value of DSCs based on ZnTCPP/C60PPy should be attributed to its prolonged injected-hole lifetime.

Photoelectron spectroscopy studies on sensitized NiO surfaces. In order to further study the configuration of different photosensitizers on the NiO surface, photoelectron spectroscopy (PES) was employed since it offers detailed information of the electronic and molecular structure by selective probing of atomic core levels and valence levels. Seven different samples were studied using PES; first the pure samples, i.e. ZnTCPP, TCPP, and C60PPy on NiO and second the mixed samples, i.e. ZnTCPP/C60PPy, C60PPy/ZnTCPP, TCPP/C60PPy, and C60PPy/TCPP on NiO (where for example the TCPP/C60PPy sample was sensitized with first TCPP and then C60PPy). In addition a sample of pure NiO was studied for energy calibration purposes and to investigate possible contamination. Aside from some residual carbon due to the sintering process, only nickel and oxygen were observed on the NiO sample.

Figure 5 shows the N 1s core level spectra and curve fits of the samples. In all samples containing TCPP and ZnTCPP two chemically inequivalent nitrogens are clearly distinguishable as two peaks in the spectra. The peaks are assigned to protonated (approx. 400.5 eV binding energy, BE) and de-protonated (approx. 398.5 eV BE) nitrogen and are characteristic for metal-free porphyrins[38]. For ZnTCPP, only one contribution to the N 1s signal is expected from the chemical structure. The presence of two chemically inequivalent nitrogens thus imply that the Zn atom is removed from the center of the porphyrin and some of the Zn-N bonds are replaced by nitrogen protonation, as previously seen for Zn-porphyrins on TiO$_2$[39]. The protons possibly originate from the acid groups in the molecule. A comparison of the N 1s spectra, see curve fits in
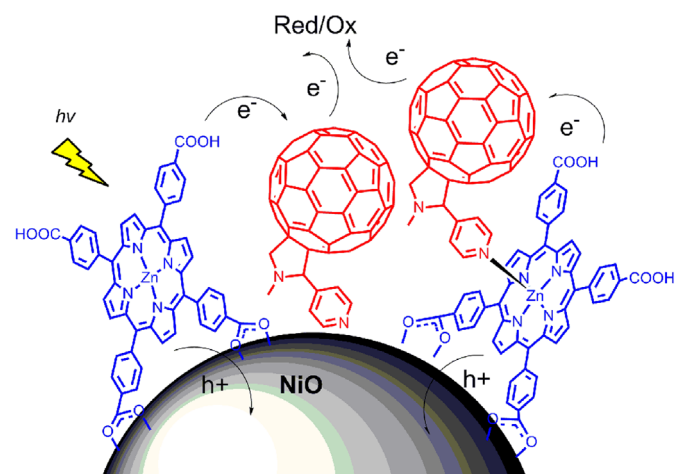

Figure 4 | Model of the surface structure and electron transfer processes of ZnTCPP/C60PPy on a NiO electrode.
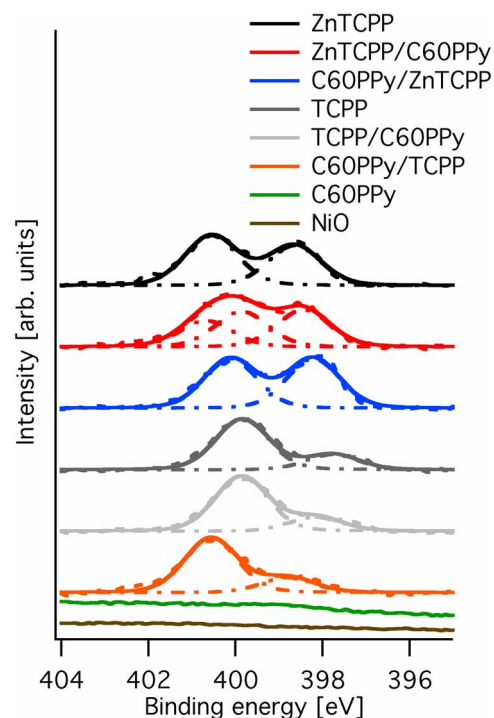

Figure 5 | N 1s core level spectra with curve fits; measured with a photon energy of 540 eV.

Figure 5, reveals a clear difference for ZnTCPP/C60PPy as compared to the others. For this sample it is no longer obvious that two species of nitrogen exist at the surface. A third species appears in between the two others (approx. 399.5 eV BE). This species has previously been reported to originate from Zn-ligated nitrogen[40]. This thus suggests that the binding configuration of ZnTCPP changes when adding C60PPy. In the case of pure C60PPy no nitrogen can be detected. This thus implies that the amount of C60PPy at the NiO surface is very low.

The valence structure of the samples can be seen in Figure 6a. In Figure 6b, the contribution from NiO has been subtracted in order to reveal the structure from Zn 3d to the valence band. For the samples containing ZnTCPP a peak corresponding to Zn 3d appears at 10.6 eV upon subtraction. The variation in BE of Zn 3d is less than 0.1 eV for the different samples indicating that the energy levels associated with the Zn atom align with the substrate. A difference in BE of 274.2 eV is observed between the C 1s and Zn 3d core levels indicating neutral zinc[39,41]. Thus, a large part of the zinc atoms are reduced from the original Zn^{2+}, which is another sign that the Zn atom is removed from the center of the porphyrin. The similar intensity of the Zn 3d peaks suggests that the amount of zinc at the surface is very alike for the different samples containing ZnTCPP.

The addition of C60PPy does not affect the amount of ZnTCPP at the NiO surface, as seen by the similar intensity of Zn 3d. However, the amount of C60PPy at the surface is very low, as seen from the N 1s. This is in agreement with absorbance measurements. There are indications that the addition of C60PPy affects the binding configuration of ZnTCPP.

The BE for the N 1s features are for example changed in the different ZnTCPP samples (Figure 5), while the Zn3d peaks line up with the substrate and are found at approximately the same BE (Figure 6b) despite the change of sample preparation. This shift between Zn3d and N1s may indicate small differences in the general binding configuration. Moreover, the variations indicate differences in the polarization between the nitrogen and the Zn atom, i.e. variations in the dipole between the NiO surface and the various nitrogens in the molecules.
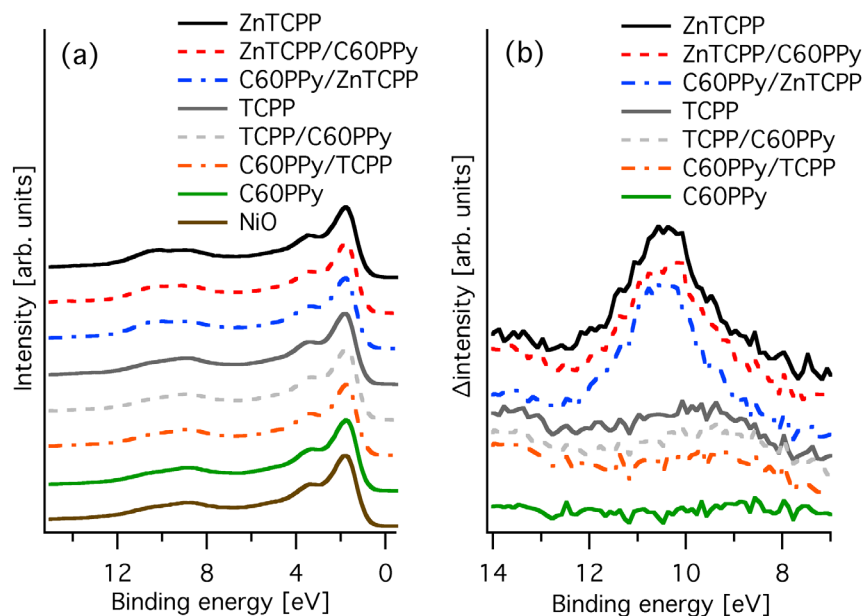
Figure 6 | (a), Valence structure and (b), the Zn 3d contribution to the valence structure obtained by subtracting the valence band of pure NiO. Measured with a photon energy of 454 eV.

In Figure 7a, the O 1s core levels for the samples are shown. Two large peaks mainly contribute to the spectra; the peak at 529.47 eV BE is attributed to NiO and the peak at approx. 531.3 eV BE to a surface layer containing Ni^{3+} such as Ni_2O_3[38]. Comparing ZnTCPP to ZnTCPP/C60PPy (and to the pure NiO) shows a feature in the spectra at a BE above Ni_2O_3. This feature is most prominent in the ZnTCPP/C60PPy sample. To deduce the origin of this feature, a spectrum subtraction was done. Subtracting O 1s measured on NiO (as measured before sensitization) reveals the oxygen in materials originating from the sensitization procedure. The subtracted spectra are presented in Figure 7b. Since C60PPy does not contain any oxygen there are no clear peaks in the spectrum after removing the substrate contribution. For all samples containing porphyrin, i.e. both ZnTCPP and TCPP, two distinct features are present in the subtracted spectra. The structure at higher BE is attributed to protonated oxygen, while the feature at lower BE is attributed to de-protonated oxygen[39,42]. The intensity of the O 1s signal (in particular that from the –OH component at higher BE) in the ZnTCPP/C60PPy sample is larger compared to the other samples. PES is a very surface sensitive technique and elements that are closer to the sample surface, i.e. further away from the NiO interface, will appear more intense in the spectra. The increased O 1s signal in combination with the presence of Zn-ligated nitrogen can thus be attributed to a change in binding configuration of ZnTCPP when adding C60PPy. In the case of ZnTCPP, the –OH feature is less prominent than in ZnTCPP/C60PPy. Thus, there are fewer carboxylic groups pointing outwards in the pure ZnTCPP sample. This indicates that ZnTCPP adsorbs to NiO lying down (with a majority of its carboxylic acid groups), as also is supported by the FT-IR data presented in Figure S13. C60PPy could cause some of the ZnTCPP molecules to adsorb to NiO standing up instead of lying down (Figure 8). This in turn means that free carboxylic groups are pointing outwards from ZnTCPP, which
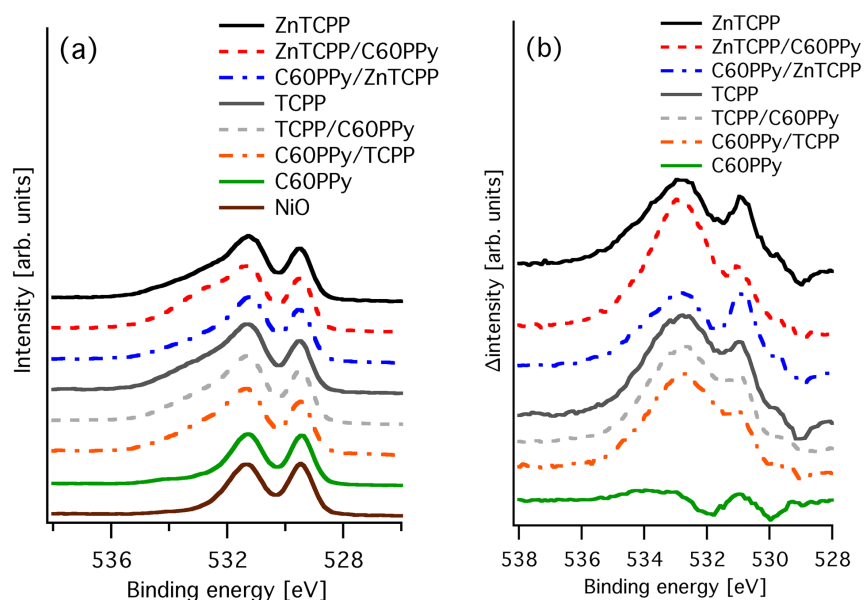

Figure 7 | (a), O1s core level spectra and (b), O 1s spectra after subtraction of O 1s from NiO. Measured with a photon energy of 758 eV.
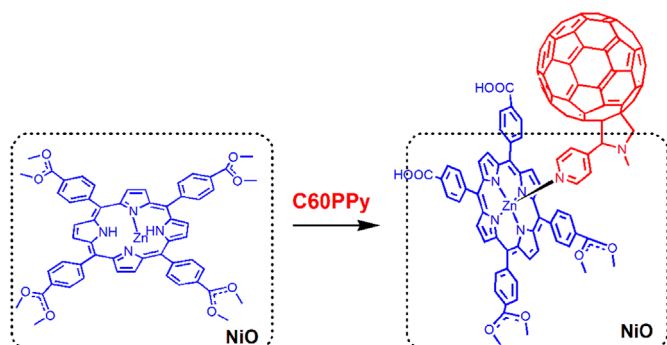
Figure 8 | Schematic drawing of the orientation of ZnTCPP on the NiO surface before and after co-sensitization with C60PPy.

explains the increase in the O 1s signal from the –OH feature. Furthermore, this means that supramolecular interaction between C60PPy and ZnTCPP is possible. This might explain why ZnTCPP/C60PPy makes the most efficient solar cell in the series.

Computational studies. To gain insight into the molecular geometry and electronic structure of the ZnTCPP/C60PPy supramolecular complex, calculations were performed. The gas-phase optimized structures were obtained using the B3LYP/6-31G(d) method as implemented in the Gaussian 09 software (Revision A.02, Gaussian Inc. Wallingford CT, 2009.). In agreement with calculations and crystal structures of similar systems, the zinc atom is pulled out of the plane of the porphyrin by 0.4 Å, upon complexation with the pyridine functionalized fullerene[43].

As expected (Figure 9), the highest occupied molecular orbital (HOMO) is located almost exclusively on the porphyrin, whereas the lowest unoccupied molecular orbital (LUMO) is on the fullerene[44]. The first unoccupied orbital belonging to the porphyrin is found at LUMO + 4 (Figure S11). There are consequently four unoccupied orbitals that can facilitate the transfer of an electron from the excited state of the porphyrin to the fullerene. Thermodynamically it is a highly favored process, with a calculated gap of 1.38 eV between the porphyrin and fullerene LUMO.

Improved photovoltaic performance and photoelectrochemical properties of devices based on $Co^{2+/3+}(dtbp)_3$ electrolyte. Due to the cobalt complexes $Co^{II/III}$ tris(4,4′-di-tert-butyl-2,2′-dipyridyl) ($Co^{2+/3+}(dtbp)_3$)-based electrolyte showing higher V_{OC} than I^-/I_3^- electrolyte in p-type DSCs[11,32], the cobalt electrolyte, **E2**, including 0.2 M $Co^{2+}(dtbp)_3$, 0.1 M $NOBF_4$ and 0.1 M $LiClO_4$ in propylene

carbonate (PC), was also employed in the ZnTCPP/C60PPy supramolecular complex sensitized NiO-based p-type DSCs. In order to get insight into the difference between the cobalt electrolyte and I^-/I_3^-, an analogous I^-/I_3^- electrolyte **E3** (0.2 M tetrabutylammonium iodide (TBAI), 0.1 M I_2 and 0.1 M $LiClO_4$ in PC) was also adopted to work with this system. The J-V curves and IPCE spectra are exhibited in Figure 10a–b. An improved efficiency was obtained by using **E2**, 0.13%, as expected with a J_{SC} of 1.5 mA·cm^{-2}, a V_{OC} of 260 mV, and a *ff* value of 0.35. Unsurprisingly, the DSCs based on **E3** showed a lower V_{OC} when compared to the devices using **E2**, 155 mV instead of 260 mV. However, the difference in redox potential between I^-/I_3^- and $Co^{2+/3+}(dtbp)_3$ is only 20 mV.

The large difference (ca. 110 mV) in V_{OC} obtained between these two redox couples must be consequently caused by other factors as well, e.g. injected hole lifetime (τ_h) or NiO Fermi level (E_F) shift. Therefore, photoelectrochemical measurements were also performed to study the effect of different electrolytes on the devices. Figure 10c shows the injected hole lifetime as a function of extracted charge (Q_{OC}); it is apparent that the hole lifetime of the device using **E2** is shorter than the device containing **E3** at a given Q_{OC}. This is may be due to the rapid hole recombination with Co^{2+} in the one-electron redox couple $Co^{2+/3+}(dtbp)_3$. The brief hole lifetime shows a passive contribution to V_{OC} in the J-V curve, from Figure 10a. From Figure 10d, which shows Q_{OC} as a function of E_F (where the E_F was approximately calculated by $E_{redox} - V_{OC}$), it can be concluded that the E_F of NiO in the device using **E2** is positively shifted about 100 mV with respect to the **E3**-based device. The enhanced V_{OC} obtained by DSCs using **E2** can be accounted for by the slight negative redox potential of the $Co^{2+/3+}(dtbp)_3$ and the positive E_F shift of NiO.

Discussion

The formation of a supramolecular complex between C60PPy and porphyrin dyes successfully improved the photovoltaic performance of p-type DSCs. Electron transfer from the porphyrin dyes to C60PPy suppresses the recombination processes between the injected holes and the reduced dyes, which increases the photovoltage and photocurrent. Using an I^-/I_3^- electrolyte, the ZnTCPP/C60PPy-based p-type DSC offered a much higher efficiency (0.09%), than the ZnTCPP-based device alone (0.02%) under simulated solar illumination. For the ZnTCPP/C60PPy-based p-type DSC, IPCE values greater than 30% and 10% were obtained at 430 nm and 560 nm, respectively. Employing the $Co^{2+/3+}(dtbp)_3$ electrolyte for the device based on ZnTCPP/C60PPy resulted in the highest efficiency (0.13%) due to the enhanced V_{OC} (260 mV). The subsequent photoelectrochemical study reveals that the positive E_F shift for NiO using the
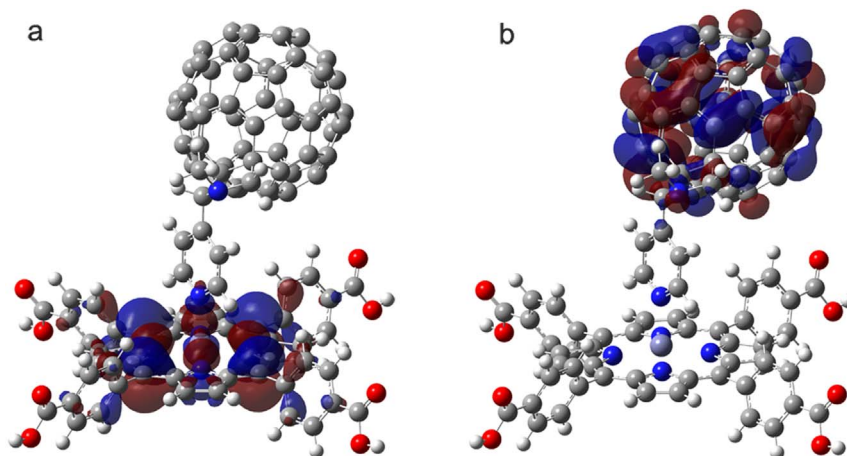

Figure 9 | HOMO (a) and LUMO (b) orbitals of the ZnTCPP/C60PPy supramolecular complex.
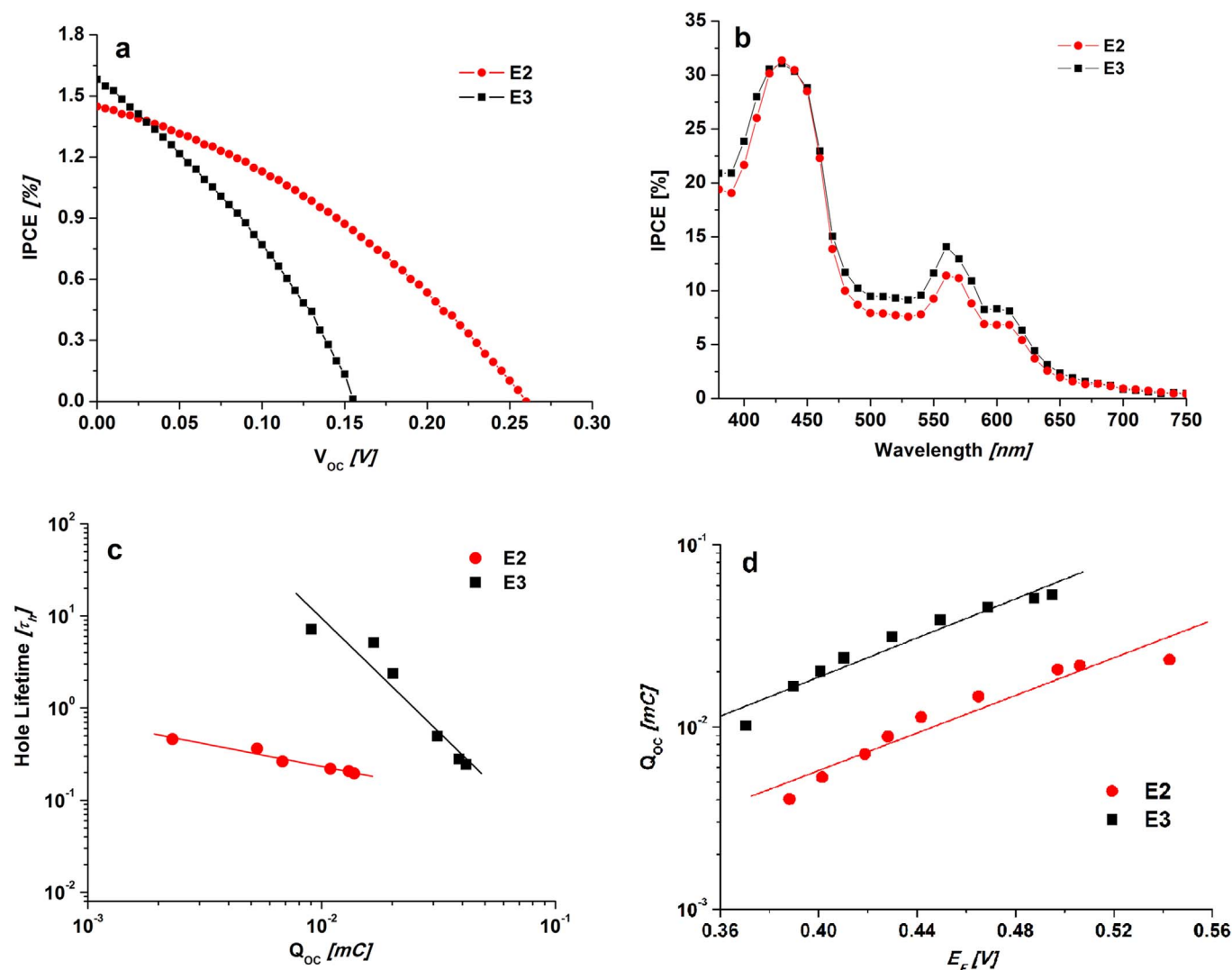
6

Figure 10 | J-V curves (a) and IPCE spectra (b) of ZnTCPP/C60PPy-based devices using E2 and E3 electrolytes; Injected hole life time as a function of extracted charge (c) and extracted charge as a function of NiO E_F (d) from ZnTCPP/C60PPy-based devices using E2 and E3 electrolytes.

$Co^{2+/3+}(dtbp)_3$ electrolyte is mainly responsible for the enhanced V_{OC} obtained in ZnTCPP/C60PPy DSCs. PES indicates that the amount of porphyrin at the surface is neither affected by the addition of C60PPy, nor is the order of sensitization. However, there are indications that the binding configuration of ZnTCPP changes when C60PPy is added, which is indicative of supramolecular interactions. The concept of combining porphyrins and C60PPy provides a facile, modular, and effective approach to improve the photovoltaic performance of p-type DSCs and will pave the road for the design of more advanced photosensitizers for p-type DSCs. Detailed electron transfer kinetic investigation of this system and further structural modifications of porphyrin and fullerene dyes are in progress.

Methods

Materials and solar cell characterization. Meso-tetra(carboxyphenyl) porphyrin (TCPP) and fullerene (C60) were purchased from Aldrich and used as received. All solvents were commercial and also used as received. ZnTCPP and C60PPy were synthesized according to literature reported methods[45,46]. NMR spectra were recorded on a Bruker AVANCE 500 MHz spectrometer. J-V characteristics were measured using a Keithley source/meter under AM 1.5 G simulated sunlight of 100 mW·cm^{-2} light intensity from a Newport 300 W solar simulator. Incident photon-to-current conversion efficiencies (IPCE) were obtained using monochromatic light from a system consisting of a xenon lamp, a monochromator and transmittance filters. Light filters were used for calibration of light intensities. Both systems were calibrated versus a certified reference solar cell (IR-filtered silicon solar cell, Fraunhfer ISE,

Freiburg, Germany). The active area of the DSCs studied was 5 mm × 5 mm. A black mask (8 mm × 8 mm) was used in the subsequent photovoltaic studies to diminish reflected light.

Photoelectrochemical measurements. Hole lifetimes for the solar cells were estimated using a green-light-emitting diode (Luxeon K2 star 5 W, λ_{max} = 530 nm) as light source. Voltage and current traces were recorded by a 16-bit resolution data acquisition board (DAQ National Instruments) in combination with a current amplifier (Stanford Research SR570). The relation between potential and charge was studied using a combined voltage decay/charge extraction method. Charge extraction measurements were carried out as follows: the solar cell was illuminated for 5 s under open-circuit conditions, the light was then switched off and the voltage was allowed to decay to a voltage V. At this voltage V, the cell was short-circuited, and the current was determined under 10 s and then integrated to obtain the charge, Q_{OC} (V). The E_F of NiO was derived from the equation $V_{OC} = E_{redox} - E_F$. Lifetimes were determined by monitoring the response in the photovoltage after a small perturbation of the light intensity.

UV-Vis measurements of dye solutions and dyed NiO films. In order to evaluate supramolecular interactions, UV-Vis absorption spectra were acquired. Due to the poor solubility of ZnTCPP and TCPP, UV-Vis absorption measurements of dyes in solution are qualitative. NiO films prepared for UV-Vis measurements were prepared by screen-printing with a literature reported NiO paste; 1 μm thick and 0.36 cm² in area[12]. The printed electrodes were heated in an oven (Nabertherm Controller P330) in ambient air atmosphere. The temperature gradient program was set to 450°C for 30 min. The sensitization time was 1 h for each compound used for the test. The final dyed NiO films were rinsed in EtOH and then dried with an air gun. UV-Vis absorbance spectra were recorded on a Lambda 750 UV-Vis spectrophotometer.

Device fabrication. Mesoporous nanostructured NiO films with a thickness of 3 μm (0.25 cm²) were prepared on FTO by screen-printing as the p-type semiconductor

electrodes. The printed NiO films were sintered at 450°C for 30 min. All films used in the study originate from the same batch. The NiO electrodes were first functionalized by sensitization in saturated ethanol solutions of TCPP or ZnTCPP for 2 h. The porphyrin-sensitized NiO films were further immersed in pure toluene or 0.1 mM C60PPy toluene solution for 16–17 h to form the pure porphyrin (TCPP or ZnTCPP)-based and porphyrin/C60PPy-based electrodes, respectively. Reference electrodes were prepared using a similar procedure but replacing C60PPy with other compounds, such as CDCA, 4-tert-butylpyridine (TBP) and C60. C60PPy/ZnTCPP electrodes were prepared by changing the sensitization order of the two compounds. All of the sensitized NiO electrodes were washed with EtOH and dried. The electrodes were then sealed with a Pt counter electrode (ca. 8.6 μg cm^{-2}) using a 25 μm thick hot-melt film (Surlyn, Solaronix) through heating the system to 120°C. Electrolytes were filled into the devices via pre-drilled holes in the counter electrodes using a vacuum procedure. Finally, the holes were sealed with a Surlyn sheet and a thin glass slide by heating.

Photoelectron spectroscopy measurements. All spectra were recorded at the undulator beamline I411 at the Swedish national synchrotron facility MAX-IV[47]. The electron take off angle was 70°. Measurements of the kinetic energies of the photoelectrons were done using a Scienta R4000 WAL analyzer. All spectra were energy calibrated relative to the O 1s core level from NiO, which was fixed to a binding energy (BE) of 529.47 eV[48]. Intensity referencing was done with respect to the O 1s from NiO.

1. Boschloo, G. & Hagfeldt, A. Spectroelectrochemistry of Nanostructured NiO. *J. Phys. Chem. B* **105**, 3039–3044 (2001).
2. Morandeira, A., Boschloo, G., Hagfeldt, A. & Hammarstrom, L. Coumarin 343-NiO Films as Nanostructured Photocathodes in Dye-Sensitized Solar Cells: Ultrafast Electron Transfer, Effect of the I$_3^-$/I$^-$ Redox Couple and Mechanism of Photocurrent Generation. *J. Phys. Chem. C* **112**, 9530–9537 (2008).
3. Qin, P. *et al.* Design of an Organic Chromophore for P-Type Dye-Sensitized Solar Cells. *J. Am. Chem. Soc.* **130**, 17629–17629 (2008).
4. Qin, P. *et al.* Synthesis and Mechanistic Studies of Organic Chromophores with Different Energy Levels for p-Type Dye-Sensitized Solar Cells. *J. Phys. Chem. C* **114**, 4738–4748 (2010).
5. Le Pleux, L. *et al.* Synthesis, photophysical and photovoltaic investigations of acceptor-functionalized perylene monoimide dyes for nickel oxide p-type dye-sensitized solar cells. *Energy Environ. Sci.* **4**, 2075–2084 (2011).
6. Zhang, X. L. *et al.* Enhanced open-circuit voltage of p-type DSC with highly crystalline NiO nanoparticles. *Chem. Commun.* **47**, 4808–4810 (2011).
7. Mishra, A., Fischer, M. K. R. & Bäuerle, P. Metal-Free Organic Dyes for Dye-Sensitized Solar Cells: From Structure: Property Relationships to Design Rules. *Angew. Chem. Int. Ed.* **48**, 2474–2499 (2009).
8. Ji, Z., Natu, G., Huang, Z. & Wu, Y. Linker effect in organic donor-acceptor dyes for p-type NiO dye sensitized solar cells. *Energy Environ. Sci.* **4**, 2818–2821 (2011).
9. Hod, I., Tachan, Z., Shalom, M. & Zaban, A. Characterization and control of the electronic properties of a NiO based dye sensitized photocathode. *Phys. Chem. Chem. Phys.* **15**, 6339–6343 (2013).
10. Yu, M., Natu, G., Ji, Z. & Wu, Y. p-Type Dye-Sensitized Solar Cells Based on Delafossite CuGaO2 Nanoplates with Saturation Photovoltages Exceeding 460 mV. *J. Phys. Chem. Lett.* **3**, 1074–1078 (2012).
11. Gibson, E. A. *et al.* A p-Type NiO-Based Dye-Sensitized Solar Cell with an Open-Circuit Voltage of 0.35 V. *Angew. Chem. Int. Ed.* **48**, 4402–4405 (2009).
12. Nattestad, A. *et al.* Highly efficient photocathodes for dye-sensitized tandem solar cells. *Nat. Mater.* **9**, 31–35 (2010).
13. O'Regan, B. & Grätzel, M. A low-cost, high-efficiency solar cell based on dye-sensitized colloidal TiO$_2$ films. *Nature* **353**, 737–740 (1991).
14. Li, L. *et al.* Visible light driven hydrogen production from a photo-active cathode based on a molecular catalyst and organic dye-sensitized p-type nanostructured NiO. *Chem. Commun.* **48**, 988–990 (2012).
15. Ji, Z., He, M., Huang, Z., Ozkan, U. & Wu, Y. Photostable p-Type Dye-Sensitized Photoelectrochemical Cells for Water Reduction. *J. Am. Chem. Soc.* **135**, 11696–11699 (2013).
16. Powar, S. *et al.* Highly Efficient p-Type Dye-Sensitized Solar Cells based on Tris(1,2-diaminoethane)Cobalt(II)/(III) Electrolytes. *Angew. Chem. Int. Ed.* **52**, 602–605 (2013).
17. Yen, Y.-S. *et al.* Arylamine-Based Dyes for p-Type Dye-Sensitized Solar Cells. *Org. Lett.* **13**, 4930–4933 (2011).
18. Chang, C.-H. *et al.* Squaraine-Arylamine Sensitizers for Highly Efficient p-Type Dye-Sensitized Solar Cells. *Org. Lett.* **14**, 4726–4729 (2012).
19. Safari-Alamuti, F. *et al.* Conformal growth of nanocrystalline CdX (X = S, Se) on mesoscopic NiO and their photoelectrochemical properties. *Phys. Chem. Chem. Phys.* **15**, 4767–4774 (2013).
20. Ji, Z., Natu, G. & Wu, Y. Cyclometalated Ruthenium Sensitizers Bearing a Triphenylamino Group for p-Type NiO Dye-Sensitized Solar Cells. *ACS Applied Materials & Interfaces* **5**(17), 8641–8648 (2013).
21. Favereau, L. *et al.* Diketopyrrolopyrrole derivatives for efficient NiO-based dye-sensitized solar cells. *Chem. Commun.* **49**, 8018–8020 (2013).
22. Ji, Z. *et al.* Synthesis, Photophysics, and Photovoltaic Studies of Ruthenium Cyclometalated Complexes as Sensitizers for p-Type NiO Dye-Sensitized Solar Cells. *J. Phys. Chem. C* **116**, 16854–16863 (2012).
23. Bessho, T. *et al.* Highly Efficient Mesoscopic Dye-Sensitized Solar Cells Based on Donor–Acceptor-Substituted Porphyrins. *Angew. Chem. Int. Ed.* **49**, 6646–6649 (2010).
24. He, J., Lindstroem, H., Hagfeldt, A. & Lindquist, S.-E. Dye-Sensitized Nanostructured p-Type Nickel Oxide Film as a Photocathode for a Solar Cell. *J. Phys. Chem. B* **103**, 8940–8943 (1999).
25. Imahori, H. & Fukuzumi, S. Porphyrin- and Fullerene-Based Molecular Photovoltaic Devices. *Adv. Funct. Mater.* **14**, 525–536 (2004).
26. Yamada, H., Imahori, H., Nishimura, Y., Yamazaki, I. & Fukuzumi, S. Enhancement of Photocurrent Generation by ITO Electrodes Modified Chemically with Self-Assembled Monolayers of Porphyrin–Fullerene Dyads. *Adv. Mater.* **14**, 892–895 (2002).
27. Yamada, H. *et al.* Photovoltaic Properties of Self-Assembled Monolayers of Porphyrins and Porphyrin-Fullerene Dyads on ITO and Gold Surfaces. *J. Am. Chem. Soc.* **125**, 9129–9139 (2003).
28. Xiao, S. *et al.* [60]Fullerene-Based Molecular Triads with Expanded Absorptions in the Visible Region: Synthesis and Photovoltaic Properties. *J. Phys. Chem. B* **108**, 16677–16685 (2004).
29. Takai, A. *et al.* Efficient Photoinduced Electron Transfer in a Porphyrin Tripod-Fullerene Supramolecular Complex via π-π Interactions in Nonpolar Media. *J. Am. Chem. Soc.* **132**, 4477–4489 (2010).
30. Tachibana, Y., Haque, S. A., Mercer, I. P., Durrant, J. R. & Klug, D. R. Electron Injection and Recombination in Dye Sensitized Nanocrystalline Titanium Dioxide Films: A Comparison of Ruthenium Bipyridyl and Porphyrin Sensitizer Dyes. *J. Phys. Chem. B* **104**, 1198–1205 (2000).
31. Tian, H. & Sun, L. Iodine-free redox couples for dye-sensitized solar cells. *J. Mater. Chem.* **21**, 10592–110601 (2011).
32. Gibson, E. A. *et al.* Cobalt Polypyridyl-Based Electrolytes for p-Type Dye-Sensitized Solar Cells. *J. Phys. Chem.C* **115**, 9772–9779 (2011).
33. Hagberg, D. P. *et al.* A novel organic chromophore for dye-sensitized nanostructured solar cells. *Chem. Commun.*, 2245–2247 (2006).
34. de Tacconi, N. R., Chanmanee, W., Rajeshwar, K., Rochford, J. & Galoppini, E. Photoelectrochemical Behavior of Polychelate Porphyrin Chromophores and Titanium Dioxide Nanotube Arrays for Dye-Sensitized Solar Cells. *J. Phys. Chem. C* **113**, 2996–3006 (2009).
35. Ooyama, Y. *et al.* Dye-Sensitized Solar Cells Based On Donor–Acceptor π-Conjugated Fluorescent Dyes with a Pyridine Ring as an Electron-Withdrawing Anchoring Group. *Angew. Chem. Int. Ed.* **50**, 7429–7433 (2011).
36. Fukuzumi, S. *et al.* Multiple photosynthetic reaction centres composed of supramolecular assemblies of zinc porphyrin dendrimers with a fullerene acceptor. *Chem. Commun.* **47**, 7980–7982 (2011).
37. D'Souza, F. & Ito, O. Supramolecular donor-acceptor hybrids of porphyrins/phthalocyanines with fullerenes/carbon nanotubes: electron transfer, sensing, switching, and catalytic applications. *Chem. Commun.*, 4913–4928 (2009).
38. Gopinath, C. S., Pandian, R. P. & Manoharan, P. T. Electronic structure of thiaporphyrins: an X-ray photoelectron spectroscopic study. *J. Chem. Soc., Dalton Trans.*, 1255–1259 (1996).
39. Rienzo, A. *et al.* X-ray absorption and photoemission spectroscopy of zinc protoporphyrin adsorbed on rutile TiO$_2$ (110) prepared by in situ electrospray deposition. *J. Chem. Phys* **132**, 084703–084706 (2010).
40. Nemykin, V. N. *et al.* Metal-free and transition-metal tetraferrocenylporphyrins part 1: synthesis, characterization, electronic structure, and conformational flexibility of neutral compounds. *Dalton Trans.*, 4233–4246 (2008).
41. Thompson, A. C. *X-ray Data Booklet 3rd ed., Center for X-Ray Optics and Advanced Light Source, 2009, Lawrence Berkeley National Laboratory, Univ. of California.*
42. Wulser, K. W. & Langell, M. A. Carboxylic acid adsorption on NiO(100) characterized by X-ray photoelectron and high resolution electron energy loss spectroscopies. *Catal. Lett.* **15**, 39–50 (1992).
43. Zandler, M. E. & D'Souza, F. The remarkable ability of B3LYP/3-21G(*) calculations to describe geometry, spectral and electrochemical properties of molecular and supramolecular porphyrin–fullerene conjugates. *C. R. Chim.* **9**, 960–981 (2006).
44. D'Souza, F. *et al.* Spectroscopic, Electrochemical, and Photochemical Studies of Self-Assembled via Axial Coordination Zinc Porphyrin−Fulleropyrrolidine Dyads. *J. Phys. Chem. A* **106**, 3243–3252 (2002).
45. Granados-Oliveros, G., Ortega, F. M., Ferronato, E. P.-M. C. & Chovelon, J.-M. Photoactivity of Metal-Phenylporphyrins Adsorbed on TiO$_2$ Under Visible Light Radiation: Influence of Central Metal. *Open Mater. Sci. J.* **4**, 15–22 (2010).
46. Wei, X.-W. *et al.* Syntheses and phtophysical properties of fulleropyrrolidines contaning photoactive units. *Fullerenes, Nanotubes and Carbon Nanostructures* **10**, 137–153 (2002).
47. Bässler, M. *et al.* Soft X-ray undulator beam line I411 at MAX-II for gases, liquids and solid samples. *J. Electron. Spectrosc. Relat. Phenom.* **101–103**, 953–957 (1999).
48. Sasi, B. & Gopchandran, K. G. Nanostructured mesoporous nickel oxide thin films. *Nanotechnology* **18**, 115613 (2007).

Acknowledgments

Author contributions

L.S. and H.T. contributed to the concept and design of the photovoltaic experiments. H.R. and J.O. contributed to design of the XPS experiments. E.G. did DFT computation. H.T. performed the synthesis of compounds and photovoltaic measurements with assistance of B.X. J.O. carried out the XPS measurements and analysis with assistance of H.R., S.K.E., R.L. and E.M.J.J. Y.H. prepared the NiO paste. G.B., J.M.G. and A.H. gave constructive suggestions and discussions. L.S., H.T., H.R. and J.O. wrote the manuscript. All authors participated in correcting manuscript and gave approval to the final version of the manuscript.

Additional information